Polar Geosci., **16**, 108–136, 2003


# Geology of eastern Mühlig-Hofmannfjella and Filchnerfjella in Dronning Maud Land, East Antarctica: A preliminary report on a Japan-Norway-Germany joint geological investigation

Masaaki Owada[1], Sotaro Baba[2], Andreas L. Läufer[3], Synnøve Elvevold[4], Kazuyuki Shiraishi[5] and Joachim Jacobs[6]

[1] *Department of Earth Sciences, Yamaguchi University, 1677–1 Yoshida, Yamaguchi 753-8512*
[2] *Department of Natural Environment, University of the Ryukyus, 1 Senbaru, Nishihara, Okinawa 903-0213*
[3] *Geologisch-Paläontologisches Institut, Johann Wolfgang Goethe-Universität, Senckenberganlage 32-34, 60054 Frankfurt am Main, Germany*
[4] *Norwegian Polar Institute, N-9296 Tromsø, Norway*
[5] *National Institute of Polar Research, Kaga, Itabashi-ku, Tokyo 173-8515*
[6] *Universität Bremen, Postfach 330440, 283340 Bremen, Germany*

(Received April 3, 2003; Accepted July 17, 2003)

***Abstract:*** The geological history of Filchnerfjella and surrounding areas (2°E to 8°E) in central Dronning Maud Land, East Antarctica, is constructed from metamorphic and igneous petrology, and structural investigations. The geology of Filchnerfjella consists mainly of metamorphic rocks accompanied by intrusive rocks. Two stages of metamorphism can be recognized in this area. The earlier stage metamorphism is defined as a porphyroblast stage (garnet, hornblende, and sillimanite stable), and the later one is recognized as a symplectic stage (orthopyroxene and cordierite stable). Taking metamorphic textures and geothermobarometries into account, the rocks experienced an early high-P/medium-T followed by a low-P and high-T stage. Partial melting took place during the low-P/high-T stage, because probable melt of leucocratic gneiss contains cordierite. The field relationships and petrography of the syenite at Filchnerfjella are similar to those of post-tectonic plutons from central Dronning Maud Land, and most of the post-tectonic intrusive rocks have within-plate geochemical features. The structural history in Filchnerfjella and surrounding areas can be divided into the Pan-African stage and the Meso to Cenozoic stage that relates to the break-up of Gondwana.

**key words**: central Dronning Maud Land, geology of Filchnerfjella, two-stage metamorphism, Pan-African magmatism, Gondwana break-up

## 1. Introduction

The nunataks of Mühlig-Hofmannfjella and western Orvinfjella (Fig. 1), a hitherto poorly known part of the Dronning Maud Land mountain range, were mapped for the first time during the Norwegian Antarctic Research Expedition (NARE) 1996–97 (Austrheim *et al.,* 1997). The area was revisited during the austral summer of 2001–

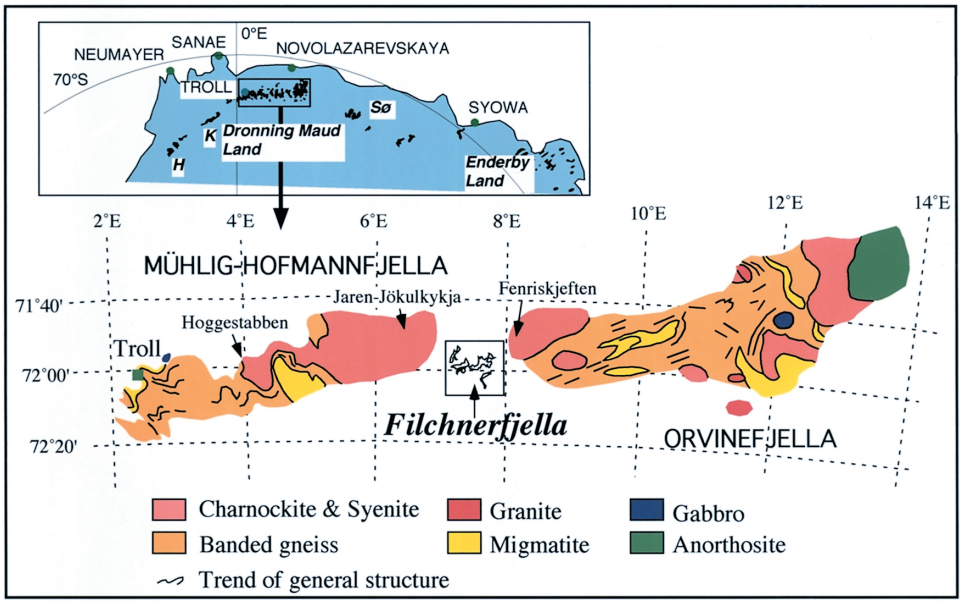


*Fig. 1. Geological sketch map of central Dronning Maud Land. Data were compiled from Ohta et al. (1990) and Jacobs et al. (1998). Sϕ: Sϕr Rondane, K: Kirwanveggen, H: Heimefrontfjella.*

02 by a Japanese-Norwegian-German joint geological expedition. This study of basement metamorphic rocks from western Orvinfjella will link the studies in western Dronning Maud Land (*e.g.,* Bucher-Numinen and Ohta, 1993; Jacobs *et al.,* 1998; Ohta, 1999; Jacobs and Bauer, 2001), with those from further east in Sør Rondane (22°–27°E), which were studied by Japanese researchers (*e.g.,* Shiraishi *et al.,* 1991).

Various workers have proposed that two tectonothermal events have affected central Dronning Maud Land (cDML), namely the Grenville-age (900–1100 Ma) and Pan-African (400–600 Ma) events (Grantham *et al.,* 1995; Moyes, 1993). Recent age determinations using SHRIMP U-Pb systematics have revealed that the Grenville-age basement was intruded by abundant Pan-African (*ca.* 500 Ma) intrusive rocks (Paech, 2001). However, precise temporal relationships involving metamorphism and deformation are still controversial.

A geological map of Filchnerfjella has not been published yet, although a reconnaissance survey was carried out by Norwegians during the field season 1996–97 (Austrheim *et al.,* 1997). According to them, the area is dominated by high-grade metamorphic rocks accompanied by voluminous intrusions of granitoids. Therefore, the area is suitable for investigating metamorphic and structural evolution. Our objective is to obtain the tectonothermal history of the area from metamorphism and related magmatism. It is stressed that the Pan-African magmatism of cDML is critical to understand the tectonic framework of Gondwana reconstruction. In particular the study could verify the kinematics of the amalgamation crustal evolution of East- and West-

Gondwana. In addition, the aim of this study was to investigate the young, Meso-Cenozoic structural architecture of cDML with regard to the break-up and fragmentation of Gondwana.

## 2. General geology of Dronning Maud Land

The coastal mountain range of cDML is exposed subparallel to, and *ca.* 200–250 km inland of the edge of the East Antarctica Ice Sheet (Fig. 1). In plate tectonic reconstructions of the Gondwana supercontinent, the DML mountain range is inferred to represent the southeastern continuation of the East African Orogen (*e.g.,* Stern, 1994; Jacobs *et al.,* 1998). The East African-East Antarctic Orogen formed as a result of collision of East and West Gondwana during the Pan-African event in the late Neoproterozoic to early Palaeozoic time. The older, Meso-proterozoic (*ca.* 1.1 Ga) basement rocks in DML were differentially reworked during the Pan-African event. Metamorphic rocks in Orvinfjella and Wohlthatmassiv (8°–14°E), eastern DML, underwent granulite facies metamorphism between 570 Ma and 515 Ma (Jacobs *et al.,* 1998). The Pan-African tectonothermal overprint was less intense in the western DML. Voluminous granitoids are exposed over a large area, from H.U Sverdrupfjella (2°E) in the west to Sør Rondane (28°E) in the east. The *ca.* 500 Ma granitoids are mainly undeformed, except from a few localized shear zones.

## 3. Geology of Filchnerfjella and surrounding area

The mountains and nunataks of Gjelsvikfjella, Mühlig-Hofmannfjella and Filchnerfjella (2°–8°E) of cDML consist of a series of post-tectonic intrusive rocks, which are emplaced into high-grade metamorphic basement rocks (Dallmann *et al.,* 1990; Austrheim *et al.,* 1997; Ohta, 1999; Jacobs and Bauer, 2001). The basement rocks comprise banded gneisses and migmatites of various compositions, whereas the igneous suite includes voluminous intrusions of charnockite, syenite, quartz-syenite, granite and several generations of dikes. The dike intrusions range in composition from granitic to gabbroic/dioritic, and granitic dikes include charnockite, aplite and pegmatite. Some of the granitoids are characterized by Fe-enriched bulk composition and contain fayalite (Ohta *et al.,* 1990).

Age dating in Gjelsvikfjella, Mühlig-Hofmannfjella and Filchnerfjella is sparse, however, two tectonothermal events are distinguished based on isotopic data. Ages around 400–500 Ma are reported by Ravich and Krylov (1964) and Ohta *et al.* (1990). Rb-Sr and Sm-Nd isotope data presented by Moyes (1993) indicated an intrusive age of 1153 Ma for granitic gneiss from Gjelsvikfjella. U-Pb dating of zircon cores from a granitic migmatite in Gjelsvikfjella yielded a protholith age of $1163 \pm 6$ Ma, whereas metamorphic zircon rims recorded a recrystallization age of $504 \pm 6$ Ma (Paulsson, 2001). Post-migmatite syenite and aplite in the same area were dated to $501 \pm 10$ Ma and $495 \pm 14$ Ma, respectively (Paulsson, 2001).

A photograph of eastern Filchnerfjella is shown in Fig. 2 and geological maps and cross sections are shown in Fig. 3. Southern Filchnerfjella proved inaccessible due to ice-falls and crevasses.

*Fig. 2. Eastern part of Filchnerfjella.*

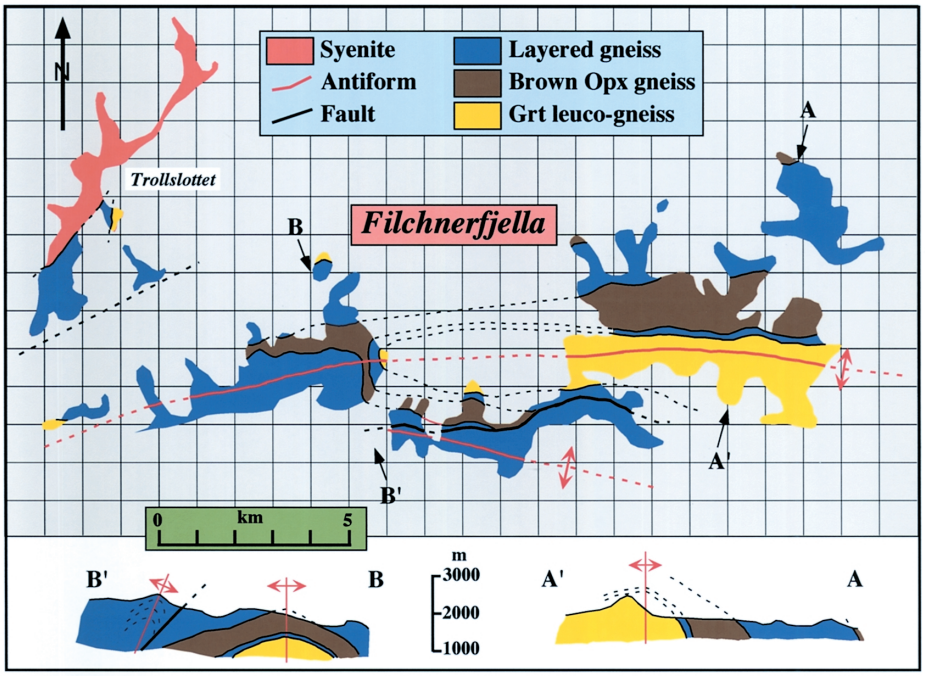


*Fig. 3. Geological map of the northern part of Filchnerfjella.*

The granulite facies metamorphic rocks in Filchnerfjella are divided into three main units from lower to higher structural level: 1) garnet-bearing leucocratic gneiss (Grt-leuco gneiss), 2) orthopyroxene-bearing brown gneiss (Opx-br gneiss) and 3) varicolored-layered gneiss (layered gneiss). A syenite stock intrudes the metamorphic rocks in the western part of Filchnerfjella, and quartz-dioritic to granitic dikes are scattered in Filchnerfjella.

The Grt-leuco gneiss is locally migmatitic. The mafic enclaves originally derived from an intrusive rock are sparsely included in the Grt-leuco gneiss. The Opx-br gneiss overlying the Grt-leuco gneiss contains dark-colored feldspar grains with weak foliations. The layered gneiss, situated at the upper structural level, consists of various colored alternating layers involving the above described Grt-leuco gneiss and Opx-br gneiss. The layered structure of this gneiss parallels the pervasive foliation.

## 4. Structural geology of Filchnerfjella and surrounding areas

In order to perform kinematic analyses and to distinguish different events in the ductilely deformed rocks in cDML, we applied continuous tracing of penetrative crystal-plastic structures, description of their orientation and nature, and recorded overprinting criteria of different deformation events. All rock types (*i.e.,* both the metamorphic units and the plutonic rocks) were studied and sampled in detail. The non-coaxial strain component was deduced from shear sense indicators in the $XZ$ plane of the finite strain ellipsoid with the principal axes $X \geq Y \geq Z$. Such indicators are, for example, S-C and shear band fabrics, rotated clasts, antithetically rotated asymmetric boudins, mica fish, or intrafolial folds (*e.g.,* Hanmer and Passchier, 1991; Passchier and Trouw, 1996).

Analysis of the younger structural architecture followed standard techniques in order to determine the fault kinematics and palaeostress states associated with brittle deformation. Measurements of fault-slip data (fault planes, striations, and lineations) were performed in all rock types. The relative block motion was deduced from kinematic indicators such as fiber steps, Riedel shears, sigmoidal brittle S-C-structures, etc. (*e.g.,* Chester and Logan, 1987; Petit, 1987; Hanmer and Passchier, 1991). Additional information on fault kinematics was derived from mapping of cogenetic structures (*e.g.,* foliation planes, folds, tension gashes, and their age relations to individual faults).

Since the areas visited around Hoggestabben, Jaren-Jøkulkyrkja, and Fenriskjevten are dominated by post-tectonic intrusive rocks and only minor proportions of metamorphic rocks are present, the studies on the Proterozoic to Early Paleozoic deformation history were mainly carried out in Filchnerfjella. The metamorphic series of Filchnerfjella and the other investigated subareas suffered polyphase deformation and metamorphism. Since no indications of pre- or syn-migmatic elements such as ptygmatic folds were observed in the banded and migmatitic gneisses, the recorded structures in the rocks must have formed after the main migmatization event. All primary structures have been obliterated by subsequent deformation. The rocks are strongly foliated and locally show a strong mineral lineation (Fig. 4).

In Filchnerfjella, several fold generations were distinguished in the gneisses. First-generation folds are isoclinal (or intrafolial) and lie within the main foliation. They are refolded by second-generation closed folds, which in turn are overprinted by relatively open third-generation folds. At one locality in Filchnerfjella, we could determine at least two highly-ductile shearing events. An older one yielded roughly top-to-NNW-directed shear senses and is pervasively observed throughout the rock. The younger is formed by distinct N-dipping (dip angle around 40°) shear zones with opposite-directed shear sense, *i.e.* approximately top-to-the-S. They cut through the

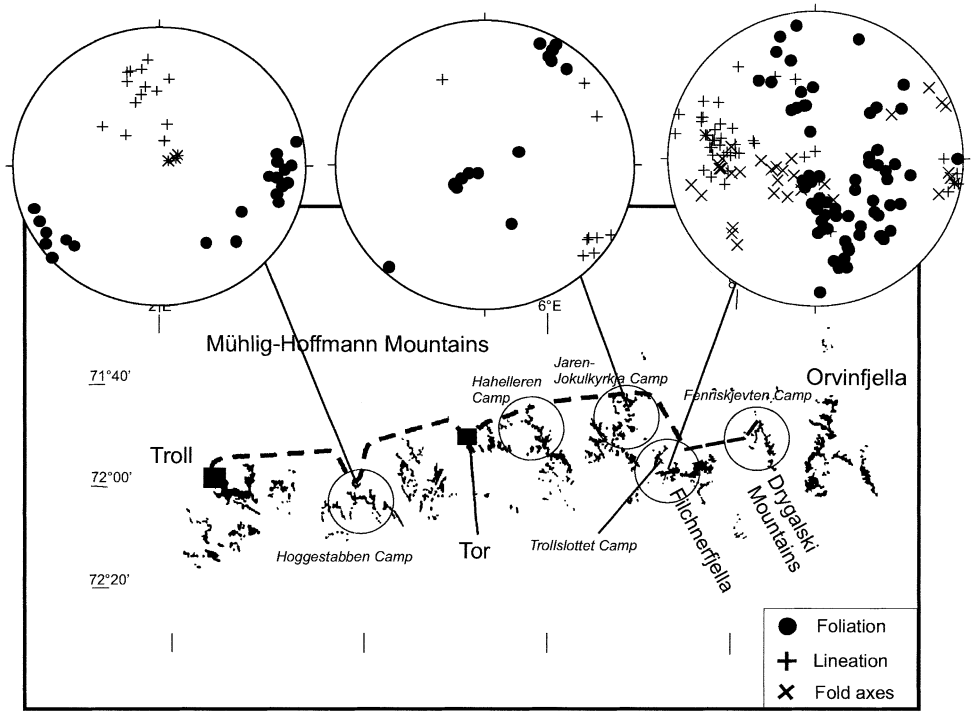


*Fig. 4. Lower hemisphere stereographic projections of the main structural elements in the metamorphic rocks of the Hoggestabben area, the Jaren-Jϕkulkyrkja area, and Filchnerfjella. The foliation planes of Filcherfjella (at the far right) lie on a great circle which defines an open fold with shallowly dipping E-W trending axis (see Fig. 6).*

aforementioned third-generation folds.

The foliation planes in Filchnerfjella define a great circle on the stereographic lower hemisphere projection (Fig. 4). This is due to spectacular large-scale folds that are present along the whole northern flank of Filchnerfjella (Fig. 5). These open folds show a slightly N- to NNW-directed vergence and are folded around shallowly dipping, roughly E-W trending axes. We observed at least two anticlines that are likely separated by a large, shallowly S-dipping fault. This fault could not be measured in detail because its location is high up on the steep northern flank of Filchnerfjella. However, due to principal geometrical fold-fault relations and the fact that this fault separates two large anticlinal structures, we assume that the fault might represent a thrust with an N-directed sense of shear. In addition, we studied the lower of the two anticlines during a short stop. The fold is offset by shallowly dipping faults that roughly parallel the large fault separating the two anticlines (Fig. 5). The fault gouges along the fault trace are recrystallized. The offset along these faults is down-dip and they thus are low-angle normal faults that were active after folding. However, we also observed large drag-folds along the fault traces. The geometrical relations of the drag folds and the faults suggest that the faults were likely initiated as thrusts and were then reactivated as extensional faults. Both the folds and the recrystallized fault zones are

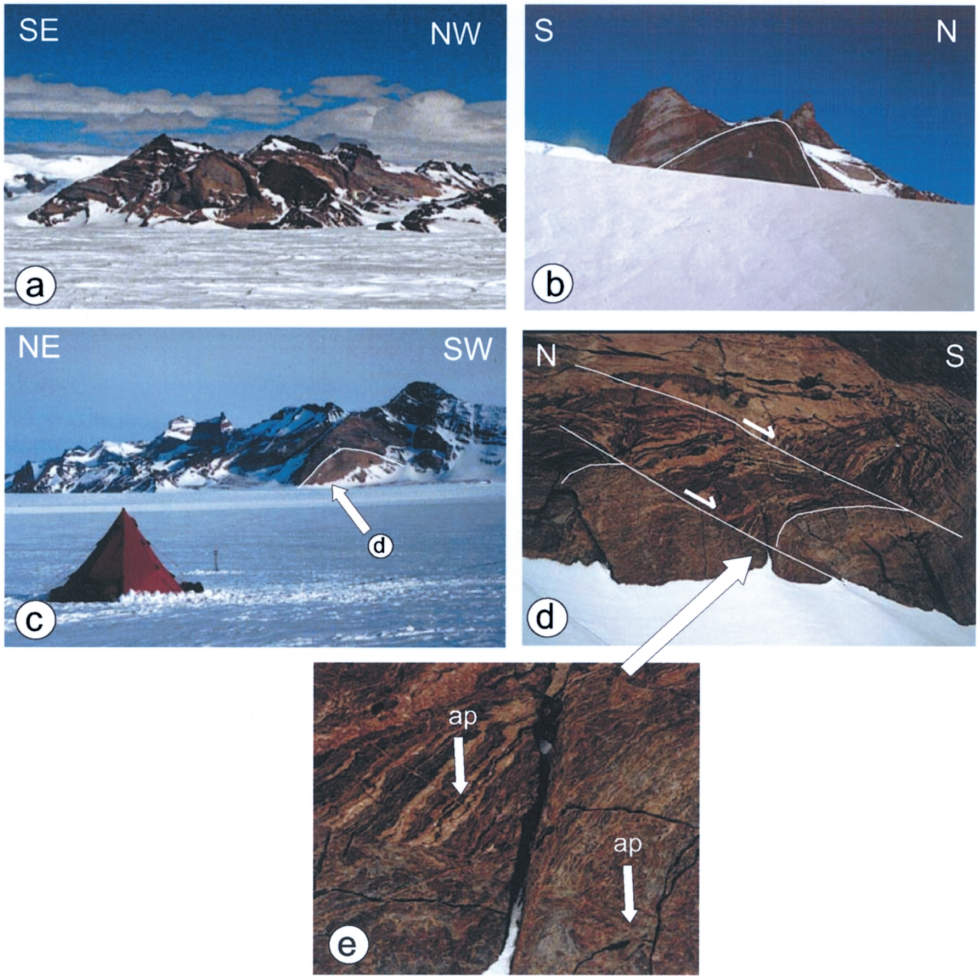


*Fig. 5. Examples of the large-scale fold and fault structures in Filchnerfjella.*
*a: View of northeastern Filchnerfjella showing one of the large-scale folds with E-W trending axes which can be traced along the whole northern flank of the range.*
*b and c: The two anticlines at the northern flank of Filchnerfjella mentioned in the text. Picture b shows the upper one of these anticlines, picture c the lower one. Both are open folds with shallowly dipping E-W axes and N- to NNW-directed vergence. The arrow in picture c indicates the location of picture d.*
*d: S-dipping low angle normal faults offsetting the lower anticline shown in picture c. The faults probably reactivate pristine thrusts genetically linked to folding.*
*e: Undeformed thin aplitic dikes (ap) cutting through the normal faults shown in picture d.*

cut by undeformed thin aplitic dikes that probably belong to the voluminous Pan-African plutonism in the area.

Structural analyses associated with brittle deformation consistently indicate the presence of a conjugate fault system in all investigated sub areas between Hoggestabben

and Fenriskjeften (Fig. 6). This is due to spectacular large-scale folds, which are present along the whole northern flank of Filchnerfjella (Fig. 5). This conjugate system is formed by the NNW-SSE trending left-lateral and WSW-ENE trending right-lateral faults. This configuration points to an approximately WNW-ESE oriented maximum horizontal palaeostress direction. It parallels the major geomorphological features and disrupts an older, pre-glacial denudation surface preserved at many places in cDML (*e.g.,* Stabben near Troll station, Hoggestabben, etc. (*cf.,* Näslund, 1997)). At northern Trollslottet, right-lateral striations overprint a not well-preserved extensional event. At the northern face of Hoggestabben, an unmetamorphsed probably Jurassic-age basic dike is preserved in one of these faults and is overprinted by the right-lateral movements. At several localities (Stålstuten in the Hoggestabben area, at Stauren in the Jaren-Jötulkyrkja area, and northern Trollslottet), we observed large thrust zones cutting through the syenite bodies (Fig. 7). These thrusts are oriented approximately NNE-SSW. The thrusting direction is either approximately WNW or ESE. They formed approximately perpendicular to the main palaeostress direction derived from the conjugate fault system. The offsets are usually on the order of only some tens to at the most a hundred meters. At Stålstuten in the Hoggestabben area, chlorite and serpentine growing on the slickenlines of these thrusts indicate that the inner fault zones reached lower low-grade temperatures during deformation. At the same locality, positive flower structure geometry in association with the conjugate fault system was observed. At Stauren in the Jaren-Jøkulkyrkja area, the internal thrust zones are strongly foliated and reveal high-strain, mylonitic to ultramylonitic deformation. These internal zones reach only a few centimeters or decimeters in thickness and

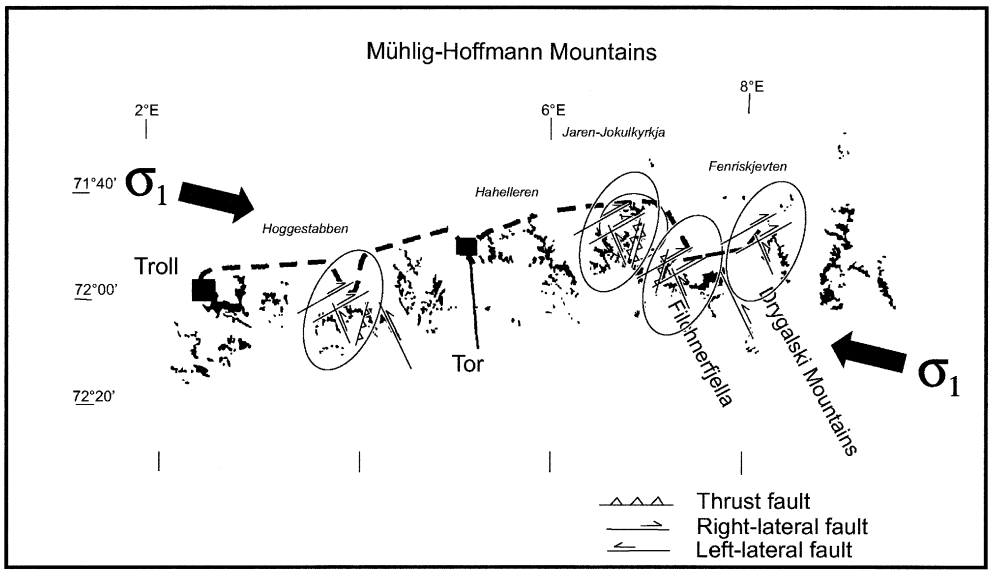


*Fig. 6. Schematic map summarizing the main brittle structures in the expedition area and the inferred regional strain ellipsoid resulting from WNW-ESE directed contraction.*

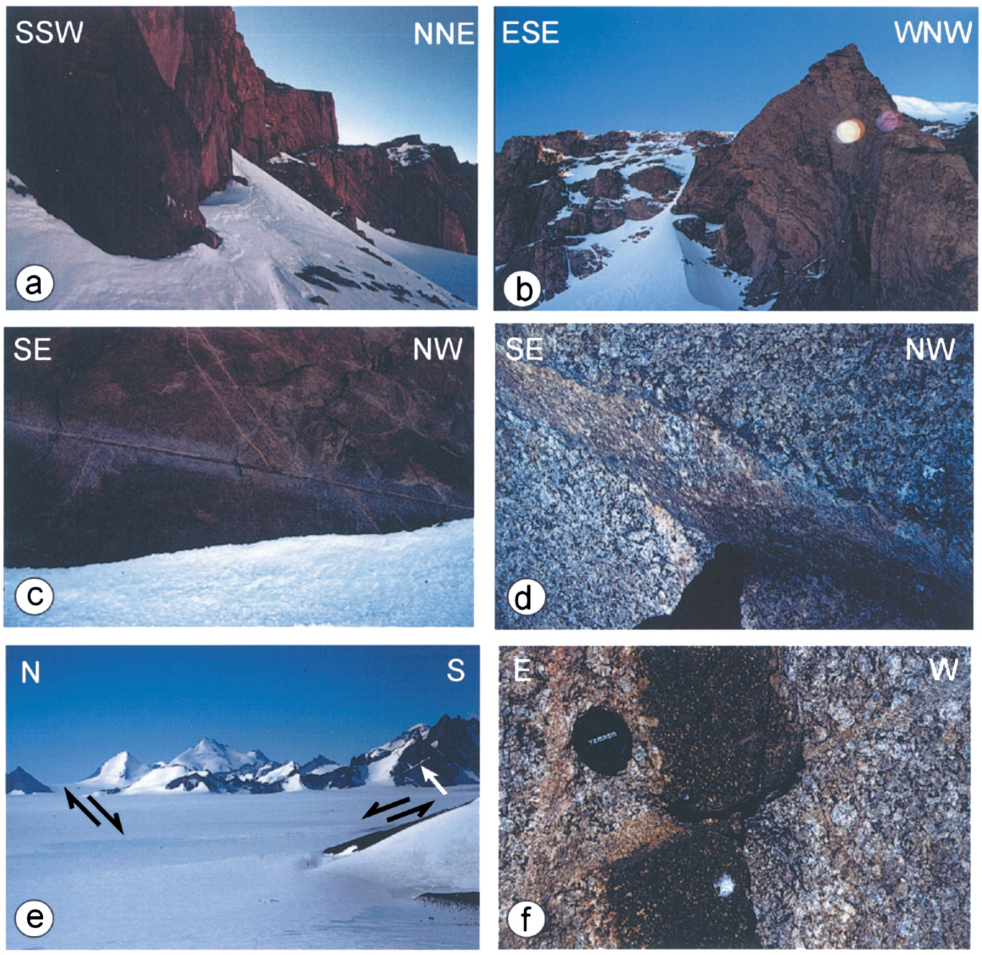


*Fig. 7. Examples for brittle structures in the expedition area.*
*a: Large-scale thrust in gneisses and magmatic rocks at Stålstuten (Hoggestabben area). The view is up the fault plane toward the WNW. b: Same thrust zone as in a. Reverse offsets are visible in the wall. c: SE-directed thrust zone in syenites at Trollslottet in Filchnerfjella. d: Inner fault zone of the example shown in picture c with strong mylonitic foliation and ductile deformation due to SE-directed thrusting. e: Large-scale conjugate fault at Hoggestabben. f: Plane view of a dike in magmatic rocks at northern Fenriskjeften. The dike is offset by a WSW-ENE trending dextral fault.*

grade into several tens of meters thick cataclastic zones with brittle deformation and finally into the undeformed plutonic rock. The shear senses in the internal fault zones were determined from rotated feldspar clasts and match the ones derived from slickensides in the brittly deformed outer zones.

## 5. Metamorphic rocks

The metamorphic rocks in Filchnerfjella are classified into seven rock types as follows:
1) Garnet-sillimanite gneiss, 2) Garnet-biotite quartzofeldspathic gneiss, 3) Orthopyroxene-bearing quartzofeldspathic gneiss, 4) Pyroxene-bearing mafic gneiss, 5) Garnet-orthopyroxene mafic gneiss, 6) Orthopyroxene-bearing brown gneiss, and 7) Metamorphosed ultramafic rocks. Relationships between the different lithological units and their associated rock types are summarized in Table 1. Representative mineral analyses of the Garnet-orthopyroxene mafic gneiss are listed in Table 2.

### *5.1. Garnet-sillimanite gneiss*

Three types of garnet-sillimanite gneisses occur as discontinuous layers alternating with feldspathic-rich layers (faint banding-type), fine alternating layers (fine layering-type), and relatively homogenous leucocratic rock (leucocratic-type) in the Grt-leuco gneiss unit (Fig. 8). These rocks appear to be restricted to the Grt-leuco gneiss unit. The former type is blackish in color with red to pale pink garnet pods (up to 1 cm), and occurs as migmatite. The latter two types have relatively massive appearance associated with garnet pods. The following mineral associations are recognized.

1) Garnet + sillimanite + cordierite + hercynite + biotite + quartz + K-feldspar + plagioclase + ilmenite.
2) Garnet + sillimanite + biotite ± muscovite + quartz + K-feldspar + plagioclase

Mineral association 1) is recognized from the faint banding-type. Garnet

*Table 1. Relationships between geological units and their associated rock types.*

| Geological unit | |
|---|---|
| Garnet-leucocratic gneiss unit | |
| | Garnet-sillimanite gneiss |
| | Garnet-biotite quartzofeldspathic gneiss |
| | Orthopyroxene-bearing mafic gneiss (as discontinuous block) |
| Layered gneiss unit | |
| | Garnet-biotite quartzofeldspathic gneiss (involving cordierite porphiroblast) |
| | Orthopyroxene-bearing quartzofeldspathic gneiss |
| | Pyroxene-bearing mafic gneiss |
| | Garnet-orthopyroxene mafic gneiss |
| | Metamorphosed ultramafic rock (as block) |
| | Orthopyroxene-bearing brown gneiss (as discrete block) |
| Brown Orthopyroxene gneiss unit | |
| | Brown orthopyroxene gneiss |
| | Garnet-bearing quartzofeldspathic gneiss |

*Table 2. Representative mineral analyses of constituent minerals of metamorphic rocks.*

| **Sample No.** | Grt-Opx mafic gneiss (02010601B) | | | | | | | |
|---|---|---|---|---|---|---|---|---|
| **Anal. No.** | 5 | 23 | 40 | 69 | 14 | 48 | 24 | 34 |
| | Opx sym | Opx sym | Grt rim | Grt core | Hbl core | Hbl in Grt | Pl | Pl |
| **$SiO_2$** (wt%) | 52.63 | 51.97 | 39.19 | 39.02 | 43.41 | 41.90 | 45.18 | 45.25 |
| **$TiO_2$** | 0.07 | 0.08 | 0.00 | 0.02 | 0.79 | 1.55 | 0.01 | 0.00 |
| **$Al_2O_3$** | 2.98 | 3.90 | 22.61 | 22.51 | 14.65 | 15.46 | 35.38 | 35.21 |
| **$Cr_2O_3$** | 0.00 | 0.05 | 0.00 | 0.00 | 0.00 | 0.02 | 0.00 | 0.00 |
| **FeO*** | 21.06 | 22.15 | 25.73 | 26.26 | 10.77 | 13.06 | 0.18 | 0.16 |
| **MnO** | 0.22 | 0.29 | 0.98 | 0.90 | 0.20 | 0.16 | 0.00 | 0.02 |
| **MgO** | 23.34 | 22.49 | 9.34 | 7.48 | 14.92 | 12.80 | 0.01 | 0.02 |
| **CaO** | 0.28 | 0.19 | 3.58 | 5.72 | 10.18 | 9.95 | 18.34 | 18.24 |
| **$Na_2O$** | 0.02 | 0.00 | 0.00 | 0.00 | 2.72 | 2.97 | 0.92 | 0.96 |
| **$K_2O$** | 0.00 | 0.00 | 0.00 | 0.00 | 0.51 | 0.50 | 0.01 | 0.01 |
| **Total** | 100.60 | 101.12 | 101.44 | 101.90 | 98.15 | 98.36 | 100.03 | 99.85 |
| **O** | 6 | 6 | 12 | 12 | 23 | 23 | 8 | 8 |
| **Si** | 1.93 | 1.91 | 2.97 | 2.97 | 6.27 | 6.12 | 2.08 | 2.09 |
| **Ti** | 0.00 | 0.00 | 0.00 | 0.00 | 0.09 | 0.17 | 0.00 | 0.00 |
| **Al** | 0.13 | 0.17 | 2.02 | 2.02 | 2.49 | 2.66 | 1.92 | 1.91 |
| **Cr** | 0.00 | 0.00 | 0.00 | 0.00 | 0.00 | 0.00 | 0.00 | 0.00 |
| **Fe** | 0.65 | 0.68 | 1.63 | 1.67 | 1.30 | 1.60 | 0.01 | 0.01 |
| **Mn** | 0.01 | 0.01 | 0.06 | 0.06 | 0.02 | 0.02 | 0.00 | 0.00 |
| **Mg** | 1.28 | 1.23 | 1.05 | 0.85 | 3.21 | 2.79 | 0.00 | 0.00 |
| **Ca** | 0.01 | 0.01 | 0.29 | 0.47 | 1.58 | 1.56 | 0.91 | 0.90 |
| **Na** | 0.00 | 0.00 | 0.00 | 0.00 | 0.76 | 0.84 | 0.08 | 0.09 |
| **K** | 0.00 | 0.00 | 0.00 | 0.00 | 0.09 | 0.09 | 0.00 | 0.00 |
| **Total cation** | 4.00 | 4.01 | 8.02 | 8.02 | 15.82 | 15.85 | 5.00 | 5.00 |
| **$X_{Mg}$** | 0.66 | 0.64 | 0.39 | 0.34 | 0.71 | 0.64 | - | - |
| **$X_{grs}$** | - | - | 0.10 | 0.15 | - | - | - | - |
| **$X_{prp}$** | - | - | 0.35 | 0.28 | - | - | - | - |
| **$X_{An}$** | - | - | - | - | - | - | 0.92 | 0.91 |

**total Fe as FeO**

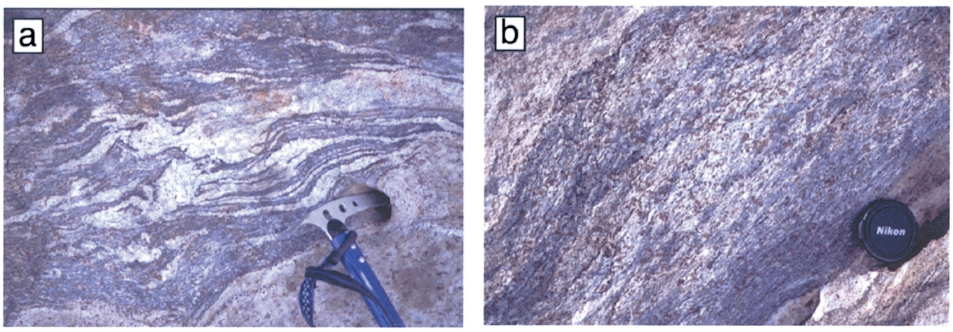


*Fig. 8. Field occurrence of the garnet-sillimanite gneiss.*
*a: Faint-banding type. Note that the garnet-sillimanite-dominant band (black) is cut by the leucocratic band. b: Layered type.*

porphyroblasts contain numerous inclusions of quartz, plagioclase, biotite, ilmenite, and hercynite. Prismatic sillimanite, hercynite, and ilmenite are mantled by cordierite. Cordierite coronas are widely developed on sillimanite margins, but locally on the garnet margin (Figs. 9a and b). Biotite forms as flakes in the matrix and as secondary grains replacing garnet. Hercynite is present in aggregates with ilmenite and sillimanite, and as inclusions in cordierite and rarely garnet. Quartz is the most dominant mineral. K-feldspar shows stringlets- and strings-type perthite structures. Plagioclase is subordinate, and occurs at grain boundaries between quartz and K-feldspar. Accessory minerals include ilmenite, zircon, rutile, and apatite.

Mineral association 2) can be seen in the fine layering-type and leucocratic-type. All minerals are finer in size compared to those of the faint banding-type. The rock has basically similar mineral associations to those of the Garnet-sillimanite gneiss, but is relatively richer in K-feldspar and muscovite (secondary). Locally, they occur as dikes cutting the foliation developed in surrounding rocks. Inclusions in garnets are sparse due to their fine grain size, but rarely, they contain spinel inclusions together with

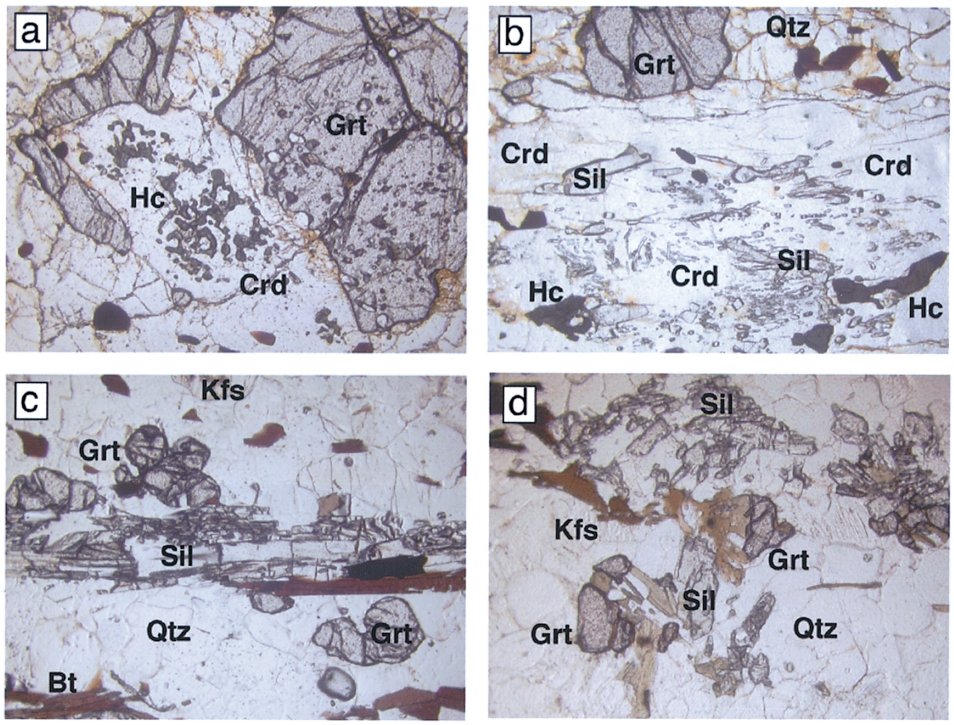


*Fig. 9. Photomicrographs of the garnet-sillimanite gneiss.*
*a: Garnet porphyroblast replaced by spinel and cordierite. Garnet porphyroblast contains numerous inclusions. Plan polarized light (PPL). Horizontal widths of photographs (a, b, c and d) are approximately 2.5 mm. b: Cordierite coronas containing hercynite, sillimanite and ilmenite (PPL). c and d: garnet and sillimanite occurrence in the layered garnet-sillimanite gneiss (PPL). Note that the sillimanites are not replaced by cordierite corona.*

plagioclase and biotite.

### *5.2. Garnet-biotite quartzofeldspathic gneiss*

Garnet-biotite quartzofeldspathic gneiss is widespread in the Layered gneiss unit and the Grt-leuco gneiss unit. The modes of occurrence and constituent minerals are highly variable such that the gneiss can be divided into three types: banded garnet-biotite gneiss, leucocratic garnet-biotite gneiss and layered garnet-biotite gneiss. In the Grt-leuco gneiss unit, the field occurrence of the banded garnet-biotite gneiss and the layered garnet-biotite gneiss is similar to that of garnet-sillimanite gneiss (Fig. 10a). In the Layered gneiss unit, banded garnet-biotite gneiss forms alternating layers associated with orthopyroxene-bearing gneiss and orthopyroxene- and clinopyroxene-bearing mafic gneiss. The leucocratic garnet-biotite gneiss occurs as discordant veins or concordant layers against the general gneissose banding. The following characteristic mineral associations are observed.

1) garnet + biotite + muscovite + quartz + K-feldspar + plagioclase + ilmenite
2) garnet + biotite + cordierite + quartz + plagioclase + K-feldspar + ilmenite
3) garnet + biotite + K-feldspar + quartz + plagioclase + ilmenite
4) garnet + biotite + hercynite + ilmenite + plagioclase + quartz

Mineral associations 2) and 3) are recognized in the banded garnet-biotite gneiss and in the layered garnet-biotite gneiss in the Layered gneiss unit. In the Grt-leuco gneiss unit, leucocratic garnet-biotite gneiss and banded garnet-biotite gneiss show associations 1), 3) and 4). Leucocratic garnet-biotite gneiss in the Opx-br gneiss unit has associations 1) and 3).

In the banded garnet-biotite gneiss, garnet occurs as porphyroblasts or in place poikiloblasts with inclusions of quartz, plagioclase, and biotite (Fig. 10b). Coarse biotite showing random orientations seems to be primary, whereas secondary biotite occurs as symplectite between garnet and coarse biotite. Cordierite, only in the Layered gneiss unit, occurs as porphyroblast with similar grain size as coexisting garnet, and does not contain any inclusions (Fig. 10c). The modal composition of quartz, plagioclase and K-feldspar varies. Part of the plagioclase shows an antiperthite texture and myrmekite is developed. Accessory minerals include ilmenite, apatite, graphite and zircon.

The layered garnet-biotite gneiss essentially shows similar mineral textures to the banded-type, except for finer grain size and garnet occurrence. Garnet occurs as subhedral grains with rounded quartz inclusions. The leucocratic garnet-biotite gneiss also has similar garnet morphology to the layered gneiss, but is relatively richer in K-feldspar (Fig. 10c). The K-feldspar is coarse grained, as well as quartz, and generally shows stringlets- to strings-structure (but parts of them show microcline structure). Small amounts of muscovite appear in the matrix.

### *5.3. Orthopyroxene-bearing quartzofeldspathic gneiss*

Orthopyroxene-bearing gneiss forms gneissose banding together with garnet-biotite quartzofeldspathic gneiss, and is widespread in the Layered gneiss unit (Fig. 11a). In the Grt-leuco gneiss unit, it occurs as thin layers alternating with garnet-biotite

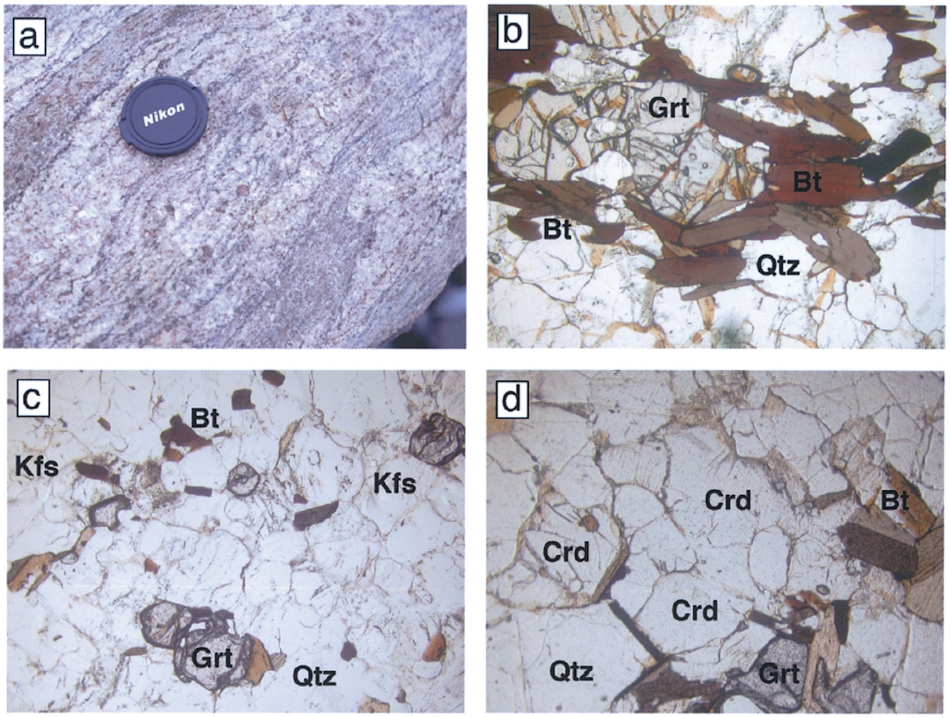


*Fig. 10. Field occurrence and photomicrographs of the garnet-biotite gneiss.*
*a: Field occurrence of layered garnet-biotite quartzofeldspathic gneiss.*
*b: Garnet porphyroblast in banded garnet-biotite quartzofeldspathic gneiss (PPL). Horizontal widths of photographs (b, c and d) are approximately 2.5 mm. c: Fine grained garnet and biotite in the leucocratic garnet-biotite gneiss (PPL). d: Cordierite-bearing garnet-biotite gneiss in the Layered gneiss unit (PPL). Note that cordierite never contains sillimanite and spinel.*

quartzofeldspathic gneiss. The constitutive minerals of the orthopyroxene-bearing quartzofeldspathic gneiss in the Grt-leuco gneiss unit are finer grain than in the Layered gneiss unit. The rock consists mainly of orthopyroxene, biotite, hornblende, plagioclase, quartz and K-feldspar. The modal variation of hornblende and biotite, and occurrence of orthopyroxene, are variable so that the gneiss can be subdivided as follows:

1) orthopyroxene (as porphyroblasts and as fine grain)＋biotite＋plagioclase＋quartz
2) orthopyroxene (as porphyroblasts and as fine mosaic grain)＋biotite＋hornblende＋plagioclase＋quartz
3) orthopyroxene (fine mosaic grain)＋biotite＋ilmenite＋plagioclase＋quartz

Mineral associations 1) and 2) are commonly recognized in the orthopyroxene-bearing quartzofeldspathic gneiss in the Layered gneiss unit. The mafic minerals show preferred orientation parallel to gneissose banding. Porphyroblastic orthopyroxene

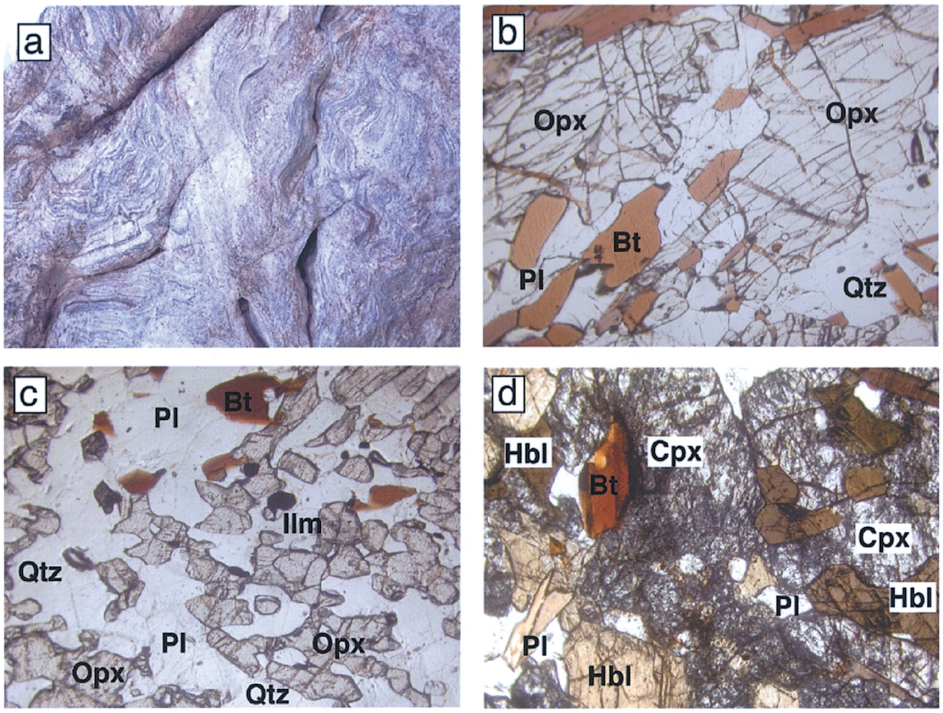


*Fig. 11. Field occurrence and photomicrographs of the orthopyroxene-bearing quartzofeldspathic gneiss and pyroxene-bearing mafic gneiss.*
*a: Field occurrence of orthopyroxene-bearing quartzofeldspathic gneiss in the Layered gneiss unit. b and c: Orthopyroxene porphyroblast and fine-grained orthopyroxene in the orthopyroxene-bearing quartzofeldspathic gneiss in the Layered gneiss unit (PPL). Horizontal widths of photographs (b, c and d) are approximately 2.5 mm. d: clinopyroxene in the pyroxene-bearing mafic gneiss (PPL).*

contains quartz and biotite inclusions (Fig. 11b). Fine mosaic orthopyroxene is finer grained than coexisting hornblende and biotite (Fig. 11c), and tends to be present in the quartz rich portions. Hornblende is brownish in color, but in places, pale green hornblende grows on the orthopyroxene margin. Accessory minerals include ilmenite, apatite, rutile and zircon.

Mineral association 3) is seen in the orthopyroxene-bearing quartzofeldspathic gneiss in the Grt-leuco gneiss unit. The gneiss normally shows granoblastic texture with medium to fine grained minerals. Orthopyroxene containing small amounts of biotite and ilmenite inclusions occurs as a fine-grained mosaic. Biotite and ilmenite are subordinate minerals compared to orthopyroxene. Plagioclase has similar grain sizes to quartz. Locally, alternating layers of garnet- and orthopyroxene-dominated layers can be seen. Accessory minerals are apatite, zircon, and rare rutile.

### *5.4. Pyroxenes-bearing mafic gneiss*

Pyroxenes-bearing mafic gneiss shows various occurrences, as a thin layer and a

continuous block in the Grt-leuco gneiss unit, and as a thick layer alternating with other lithologies in the Layered gneiss unit. Mineral associations are highly variable due to modal variation of clinopyroxene, orthopyroxene, hornblende, and biotite. The briefly classified mineral assemblages of pyroxene-bearing mafic gneiss are as follows:

1) orthopyroxene + clinopyroxene ± hornblende + biotite + plagioclase ± quartz
2) orthopyroxene + biotite ± hornblende + plagioclase + quartz
3) clinopyroxene + hornblende ± biotite + plagioclase ± quartz

There are no distinctive relationships between the mineral associations and field occurrence. However, pyroxene-bearing mafic gneiss occurring as a block tends to show granoblastic textures without any significant preferred orientation. In the Layered gneiss unit, orthopyroxene occurs as porphyroblasts and as small grains. The former occurs in the rock that consists of a large amount of biotite, and the latter of hornblende. In the hornblende-rich lithology, clinopyroxene occurs in the major phase instead of orthopyroxene. Coarse-grained clinopyroxene locally includes hornblende and plagioclase (Fig. 11d). Plagioclase dominates in all the lithologies, and locally shows antiperthitic structures. Secondary cummingtonite replaces orthopyroxene. Accessory minerals are ilmenite and apatite.

### *5.5. Garnet-orthopyroxene mafic gneiss*

This gneiss is observed in the Layered gneiss unit as a layer (Figs. 12a and b), and in the Grt-leuco gneiss unit as a mafic enclave (as a continuous block) (Fig. 12c). Two types of Grt-Opx mafic gneisses, a banded type and a garnet-pod type, can be seen in the Layered gneiss unit. The banded-type is locally intruded by orthopyroxene-bearing pegmatite (Fig. 12b). The mafic enclave in the Grt-leuco gneiss unit corresponds to the banded-type.

The banded type shows granoblastic textures with garnet, hornblende, orthopyroxene and plagioclase as major constituents (Figs. 13a and b). Biotite, clinopyroxene and quartz are subordinate phases. Compositional bands formed by alternating garnet-hornblende-, garnet-orthopyroxene-, and hornblende-orthopyroxene-dominant bands are developed. Garnet occurs as medium-grained subhedral crystals containing tiny hornblende, plagioclase and ilmenite inclusions. Hornblende is subhedral and brownish in color. Orthopyroxene occurs as fine- to medium-grained subhedral crystals (Figs. 13a and b). Garnet and hornblende are coarser in grain size than other phases, and orthopyroxene is subordinate in grain size. Rarely, symplectic orthopyroxene and hornblende replace the garnet. Plagioclase is abundant in all bands. Accessory minerals are ilmenite and apatite.

The garnet-pod type commonly contains garnet porphyroblast (up to 30 mm), pale brown hornblende, symplectic orthopyroxene, plagioclase, biotite and spinel with trace amounts of quartz. Garnet porphyroblasts have tiny inclusions of hornblende, plagioclase, ilmenite and spinel (Fig. 13c). Pale brown hornblende forms coarse-grained subhedral crystals. Orthopyroxene only occurs as wormy symplectic crystals and replaces the garnet and hornblende margin together with plagioclase (Fig. 13d). Plagioclase encloses orthopyroxene poikilitically. Spinel occurs as aggregates surrounded by An-rich plagioclase, and locally as inclusions within garnet. Rarely, orthopyroxene

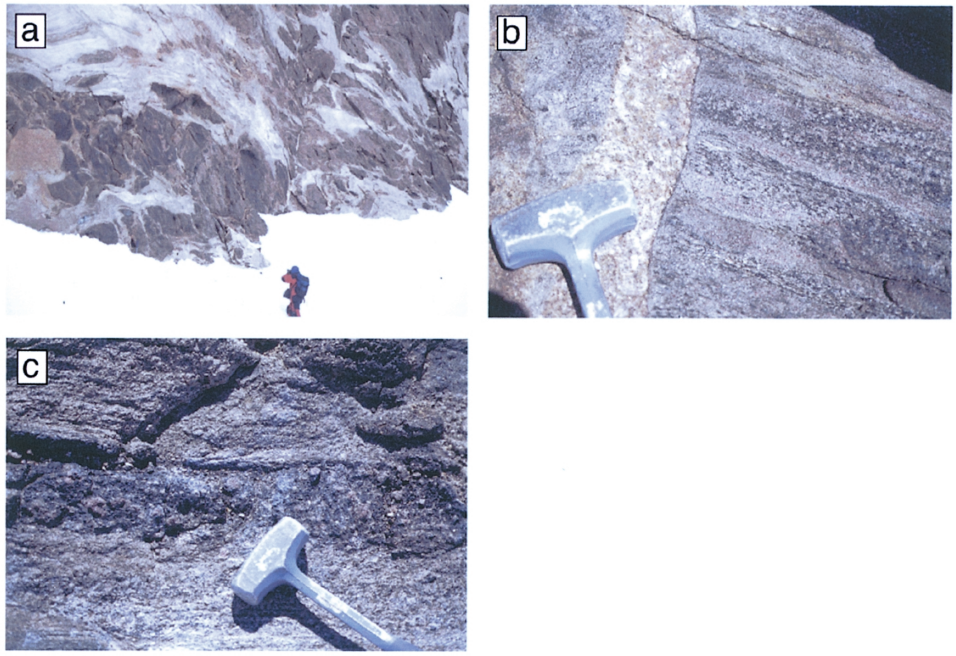


*Fig. 12. Field occurrences of the garnet-orthopyroxene mafic gneiss.*
*a: Mafic gneiss occurs as continuous blocks and enclaves in the Grt-leuco gneiss. b: Garnet-orthopyroxene mafic gneiss occurs as layer in the Layered gneiss unit. Note that the gneissose banding is cut by the orthopyroxene-bearing pegmatic vein. c: Alternation of garnet-orthopyroxene-dominant and garnet-hornblande-dominant band (banded-type).*

symplectite has spinel inclusions. Biotite occurs as elongated lath-shaped crystals in orthopyroxene-plagioclase coronas as a secondary mineral. Accessory minerals are ilmenite and apatite.

### *5.6. Orthopyroxene-bearing brown gneiss*

Orthopyroxene-bearing brown gneiss is widespread in the Opx-br gneiss unit, although this gneiss occurs as a small block in the Layered gneiss unit. The gneiss is commonly homogeneous, but weekly foliated (Fig. 14a). It consists of K-feldspar, quartz, plagioclase, orthopyroxene, hornblende, garnet, ilmenite and rare olivine (Fig. 14b). Large amounts of K-feldspar and quartz are coarser grained than the other phases. Coarse K-feldspar has stringlets to strings perthite structures. Plagioclase is locally antiperthitic. Orthopyroxene, showing green to pale green pleochroism, forms medium-grained anhedral crystals with round inclusions of quartz. Garnet contains ilmenite and quartz inclusions. Orthopyroxene and garnet are observed to be in contact. Hornblende occurs as medium-grained anhedral crystals, and has similar shapes to orthopyroxene. Sporadically, tiny laths of biotite occur. Fine-grained anhedral olivine can be seen in the orthopyroxene- and hornblende-rich portions and in the matrix. Accessory minerals are ilmenite, apatite and zircon.

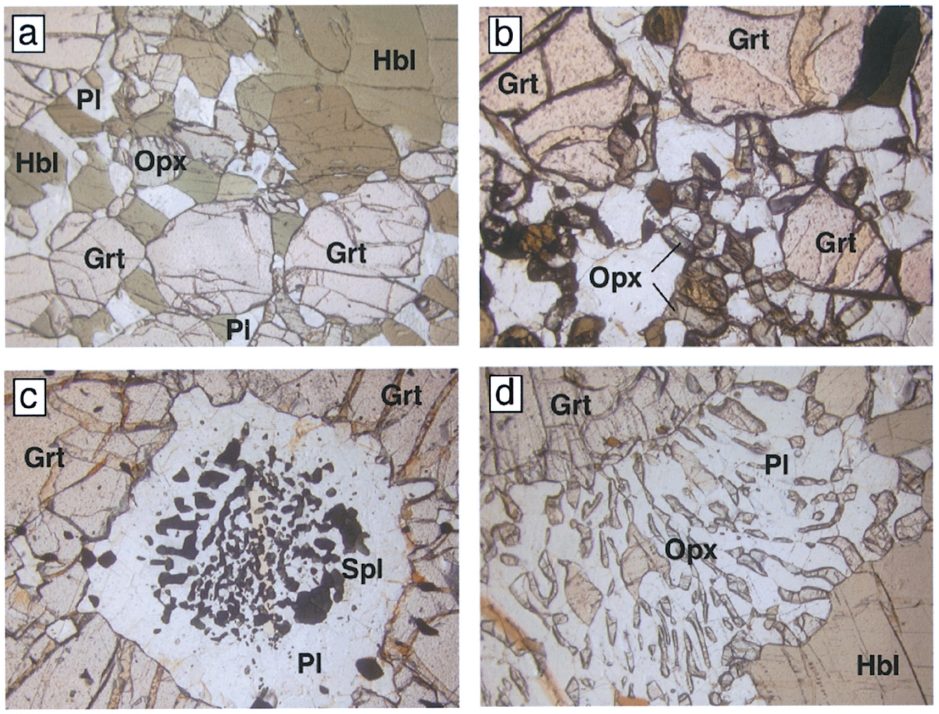


*Fig. 13. Photomicrographs of the garnet-orthopyroxene mafic gneiss.*
*a: Garnet and hornblende occur as porphyroblast, and orthopyroxne only occurs as minor phase (PPL). Horizontal widths of photographs (a, b, c and d) are approximately 2.5 mm.*
*b: Fine-grained orthopyroxene developed (PPL). c: Garnet contains spinel and plagioclase inclusion (PPL). d: Garnet and hornblende replaced by wormy orthopyroxene symplectites (PPL).*

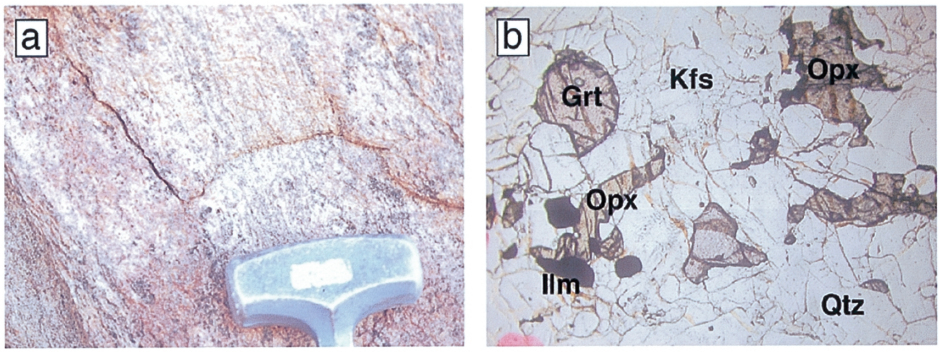


*Fig. 14. Field occurrence and photomicrographs of the orthopyroxene-bearing brown gneiss in the Opx-br gneiss unit.*
*a: Field occurrence of orthopyroxene-bearing brown gneiss. b: Photomicrographs of typical orthopyroxene-bearing brown gneiss (PPL). The horizontal width of the photograph is approximately 2.5 mm.*

### *5.7. Metamorphosed ultramafic rock*

Metamorphosed ultramafic rock was found as an exotic block in the garnet- and orthopyroxene-bearing gneisses at one locality in the Layered gneiss unit (Fig. 15a). Several occurrences can be seen in the far-off distance, but only one locality is examined.

The rock consists of orthopyroxene, clinopyroxene, olivine, hornblende (pargasitic), biotite and ilmenite. Orthopyroxene and clinopyroxene are present as medium-grained, anhedral crystals surrounded by hornblende (Fig. 15b). Fine-grained olivine shows altered margins and is rimmed by hornblende. The pale green hornblende is the dominant phase in this rock. In places, biotite occurs as lath shape grains. Ilmenite is present as an accessory mineral.

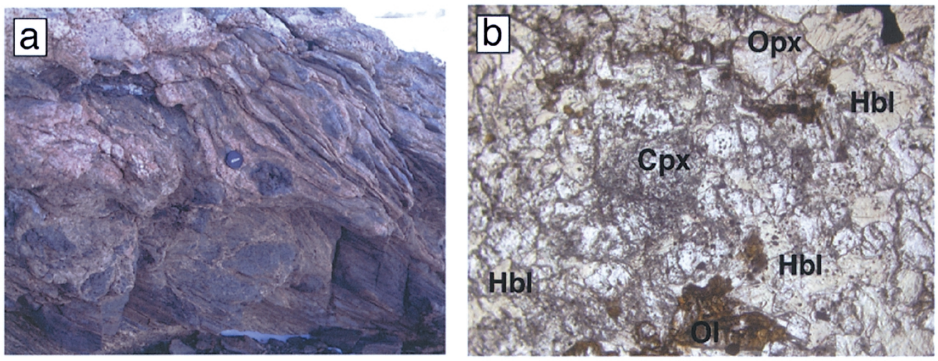


*Fig. 15. Field occurrence and photomicrographs of the metamorphosed ultramafic rock in the Layered gneiss unit.*
*a: Field occurrence of the metamorphosed ultramafic rock. b: Photomicrographs of typical metamorphosed ultramafic rock (PPL). The horizontal width of the photograph is approximately 2.5 mm.*

## 6. Intrusive rocks

The intrusive rocks exposed in this area are classified into the following lithologies: (1) syenite, (2) quartzdiorite and granite, and (3) pegmatite to aplite.

### *6.1. Syenite suite*

The syenite suite is exposed on Trollslottet, the western part of Filchnerfjella, as a stock (Figs. 3 and 16a). This suite is made up of brown syenite accompanied by a pink to gray pegmatite to aplite and a fine-grained dark gray dioritic enclave. The pink to gray pegmatite to aplite occurs as a dike intruding into the brown syenite, where a bleached zone is present along the dike margin (Fig. 16b).

The syenite is massive and coarse-grained, and consists mainly of K-feldspar (perthite), hornblende, orthopyroxene, clinopyroxene, biotite, plagioclase and quartz. Apatite, zircon, ilmenite and allanite are accessory minerals (Fig. 17a). Euhedral K-feldspar is up to 5 cm, whereas plagioclase constitutes euhedral crystals up to 5 cm in size. Hornblende and biotite surround clinopyroxene and orthopyroxene, respectively.

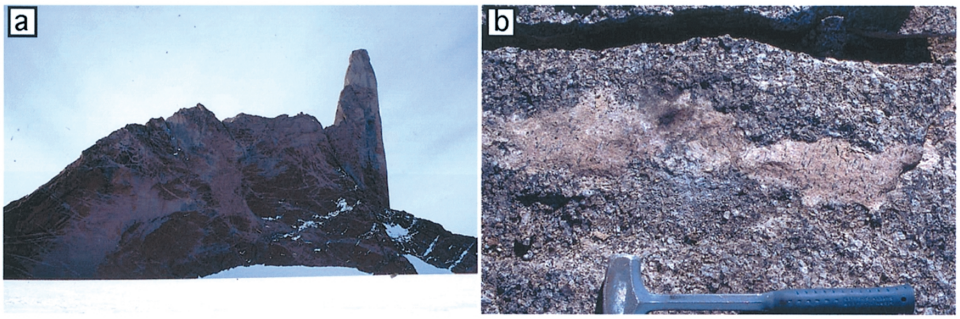


*Fig. 16. Field occurrence of the syenite suite.*
*a: Syenite stock at Trollslottet. The height of the nunatak is about 500 m above the surface of the snowfield. b: The bleached zone along the pink aplite dike.*

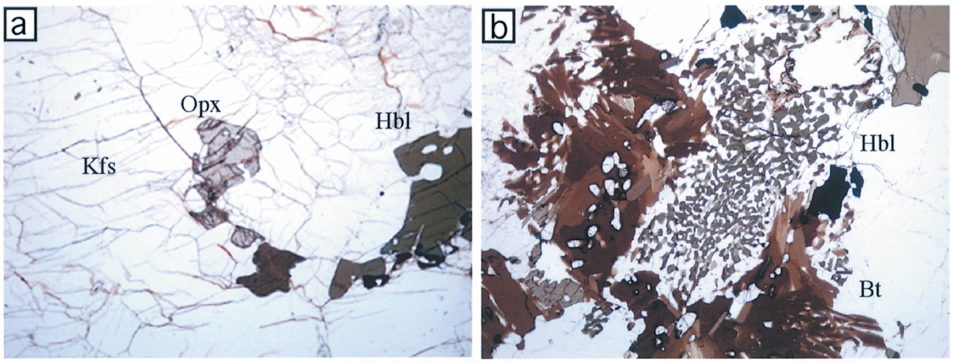


*Fig. 17. Photomicrograph of the syenite.*
*a: Orthopyroxene coexists with feldspars (PPL). Horizontal widths of photographs (a and b) are approximately 2.5 mm. b: Green hornblende and quartz symplectite surrounded by biotite flaks, in the bleached zone of the syenite (PPL).*

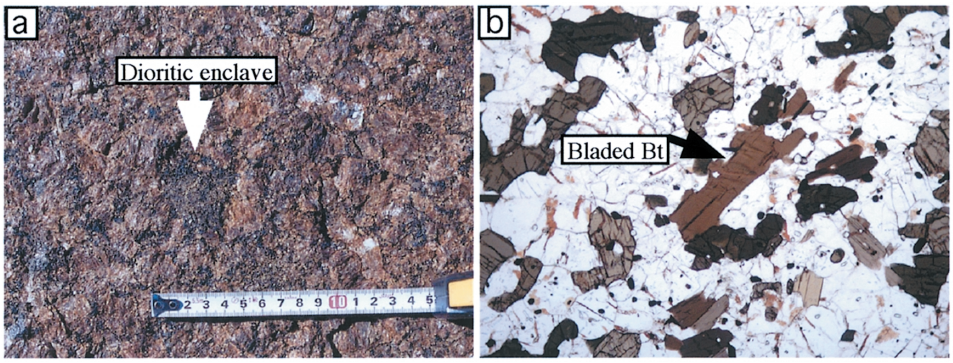


*Fig. 18. Field occurrence and photomicrograph of the dioritic enclave.*
*a: Field occurrence of the spherule-shape dioritic enclave. b: Photomicrograph of the dioritic enclave (PPL). The horizontal width of the photograph is approximately 1.2 mm. Note: occurrence of the bladed biotite.*

These textures are associated with small-grained quartz, suggesting that pyroxenes reacted with melt to produce those hydrous minerals and quartz during a cooling stage.

Well-developed bleaching zones (decoloration) are present around pegmatites and aplites, which intrude into the dark colored syenite. The bleaching is related to hydration of pyroxenes and sericitization of plagioclase. The mafic minerals in the bleached zone are only hydrous minerals such as hornblende and biotite but not pyroxenes (Fig. 17b). From the textural point of view, the bleached zone was probably formed by fluid hydration derived from the pegmatite or the aplite dikes.

The dioritic enclave has an almost spherical shape and is 5 to 50 cm in diameter (Fig. 18a), and locally includes into the host syenite. The enclave consists of hornblende, biotite, plagioclase, K-feldspar and quartz with apatite, zircon and opaque minerals (Fig. 18b). The biotite grains show bladed shapes (Fig. 18b).

### *6.2. Quartzdiorite and granite*

The quartzdiorite and granite intrude into the metamorphic rocks as dikes at the eastern part of the Filchnerfjella, and are fine- to medium-grained and display weak foliation. The dikes locally occur as composite dikes, forming a banded structure (Fig. 19).

The quartzdiorite consists mainly of plagioclase, biotite, hornblende, K-feldspar and quartz with apatite, zircon and opaque minerals. The pervasive foliation defined by orientation of the mafic minerals, such as biotite and hornblende, is parallel to the intrusive direction. The granite is relatively coarse-grained compared to the quartzdiorite, and is composed of plagioclase, quartz, K-feldspar and biotite.

### *6.3. Pegmatite to aplite*

The pegmatite to aplite occurs as dikes throughout the studied area. The dikes are up to 20 cm in width, composed of various sizes of grains, and have hydrous impact on the host rocks with considerable frequency (Fig. 17b). The mineral assemblages of the pegmatite to aplite include quartz, K-feldspar and plagioclase, with biotite and horn-

*Fig. 19. Occurrence of the composite dike (quartzdiorite in dark color and granite in light color). The thickness of the composite dike is approximately 2 m.*

blende.

## 7. Whole-rock chemical compositions of the intrusive rocks

The whole-rock chemical analyses of the described intrusive rocks were determined by XRF at the Center of Instrumental Analysis, Yamaguchi University. We chose homogeneous samples for the whole-rock chemical analyses. The results are listed in Table 3.

The syenite has 61 and 63 wt% $SiO_2$ and is characterized by high $K_2O$ and Ba with low MgO. The compositions of the dioritic enclave and the quartzdiorite (Table 3) are characterized by high $K_2O$ and Ba in spite of relatively low $SiO_2$ contents compared to the syenite. The granite and the aplite possess higher $SiO_2$ and lower FeO and MgO than the other rock types.

In the total alkali ($Na_2O+K_2O$) vs. $SiO_2$ diagram, the analyzed samples plot in the field of alkaline rock-series defined by Cox *et al.* (1979). Figure 20 shows the $SiO_2$ vs. $K_2O/Na_2O$ diagram, and also illustrates the compositional fields of the syenite and

*Table 3. Major and trace element analyses of intrusive rocks from Filchnerfjella.*

| Lithology | Qd | Gr | Sy | Sy | Apl | Di-enclave |
|---|---|---|---|---|---|---|
| Sample No. | 02010204A | 02010204B | 02010402A | 02010402B | 02010402C1 | 02010402D |
| $SiO_2$(wt%) | 56.27 | 71.35 | 62.93 | 61.14 | 74.22 | 54.65 |
| $TiO_2$ | 2.06 | 0.33 | 1.13 | 1.21 | 0.11 | 1.91 |
| $Al_2O_3$ | 15.30 | 15.33 | 16.23 | 15.65 | 13.68 | 15.50 |
| $Fe_2O_3$ | 8.41 | 2.62 | 6.52 | 6.32 | 1.59 | 9.05 |
| MnO | 0.13 | 0.03 | 0.08 | 0.08 | 0.02 | 0.10 |
| MgO | 2.54 | 0.37 | 1.41 | 1.34 | 0.15 | 2.27 |
| CaO | 4.65 | 1.26 | 3.04 | 3.22 | 1.76 | 4.79 |
| $Na_2O$ | 3.00 | 2.59 | 3.32 | 3.30 | 3.27 | 3.32 |
| $K_2O$ | 5.89 | 6.78 | 5.86 | 6.45 | 4.92 | 6.41 |
| $P_2O_5$ | 0.54 | 0.02 | 0.07 | 0.03 | 0.02 | 0.50 |
| Total | 98.79 | 100.68 | 100.59 | 98.74 | 99.74 | 98.50 |
| Ba (ppm) | 3396 | 1256 | 2819 | 2678 | 467 | 2874 |
| Nb | 35 | 9 | 25 | 30 | 10 | 45 |
| Rb | 216 | 264 | 123 | 150 | 194 | 147 |
| Sr | 1451 | 184 | 672 | 713 | 243 | 779 |
| V | 148 | 26 | 80 | 88 | 9 | 150 |
| Y | 238 | 35 | 71 | 129 | 80 | 266 |
| Zn | 164 | 59 | 95 | 111 | 52 | 147 |
| Zr | 543 | 187 | 459 | 613 | 188 | 569 |

Qd: quartzdiorite, Gr: granite, Sy: syenite, Apl: aplite, Di-enclave: dioritic enclave.

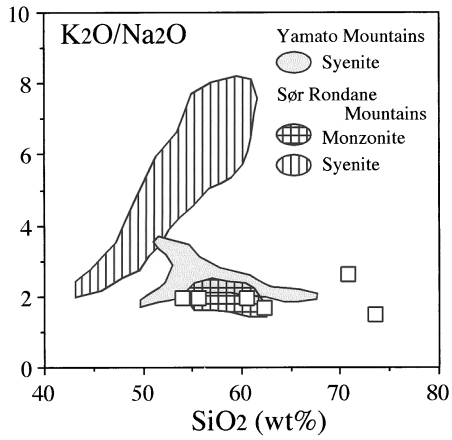


*Fig. 20. $K_2O/Na_2O$ vs. $SiO_2$ diagram of the rocks from Filchnerfjella and the Yamato and Sφr Rondane mountains. Data of the syenite and the monzonite of the Yamato and Sφr Rondane mountains are quoted from Shiraishi et al. (1983), Sakiyama et al. (1988) and Tainosho et al. (1992).*

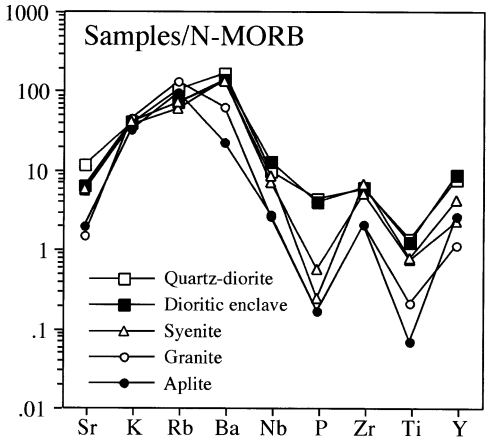


*Fig. 21. N-MORB normalized incompatible element patterns for the rocks from Filchnerfjella.*

monzonite suites from the Sør Rondane and Yamato Mountains. The $K_2O/Na_2O$ ratios of the rocks from Filchnerfjella are constant with increasing $SiO_2$ content. This trend is similar to that of the syenite suite in the Yamato Mountains and the monzonite suites in the Sør Rondane Mountains, respectively, but is different from that of the syenite suite in the Sør Rondane Mountains.

The spider diagram normalized to N-MORB values indicates that the analyzed samples show similar patterns characterized by high concentrations of K, Rb and Ba and no negative Nb anomalies regardless of their lithologies (Fig. 21). Especially, the quartzdiorite and the dioritic enclave show almost the same patterns, suggesting that these rocks were derived from a similar parental magma. The syenite, granite and aplite show negative P and Ti anomalies due to fractionation of apatite and Fe-Ti oxide as early crystallized phases.

## 8. Discussion

### *8.1. Metamorphism*

The microscopic mineral textures and field relationships can be used to reconstruct a preliminary metamorphic history for Filchnerfjella. These are summarized below.

1) Symplectic orthopyroxene grows at the expense of garnet and hornblende porphyroblasts in the garnet-orthopyroxene mafic gneiss.

2) In the garnet-sillimanite gneiss, cordierite includes sillimanite, hercynite, and ilmenite, and the garnet locally contains hercynite inclusions. These textures indicate

that the mineral association of garnet—hercynite—sillimanite was stable at an early stage and cordierite at a later stage.
3) Field relations between the faint banding-type garnet-sillimanite gneiss and the leucocratic garnet-sillimanite/garnet-biotite gneiss indicate that they might be associated with the partial melting of aluminous metasediment. In addition, the probable melting of garnet-bearing leucocratic gneisses can be seen in various parts of the Filchnerfjella as dikes.

As described above, two metamorphic stages can be recognized: the early porphyroblast stage (garnet, hornblende and sillimanite stable) and the later symplectite stage (orthopyroxene and cordierite stable). The following reactions can be inferred from the early stage to the later stage.

garnet + quartz = orthopyroxene + plagioclase.
hornblende + quartz = orthopyroxene + plagioclase + $H_2O$.
garnet + sillimanite + quartz = cordierite.

These reactions are promoted by decreasing the pressure and/or increasing the temperature. Figure 22 shows a preliminary P-T estimation of both stages based on experimentally calibrated geothermobarometers for the garnet-orthopyroxene mafic gneiss (garnet-pod type). Garnet-hornblende and hornblende-plagioclase geothermometers and garnet-hornblende-plagioclase-quartz equilibria were applied for the early stage, garnet-orthopyroxene geothermometry and garnet-orthopyroxene-plagioclase-quartz equilibria for the later stage. Details about re-equilibration effects on Fe-Mg exchange during the retrograde stage will be discussed elsewhere. The results indicate the following P-T conditions: high-P/medium-T at an early stage and low-P and high-T at a later stage. Cordierite in the garnet-sillimanite gneiss and symplectic orthopyroxene might be during decompression in the clockwise loop. In the course of decompression, partial melting may occur, because the probable melt of leucocratic gneiss contains cordierite. Further detailed studies of the formation of porphyroblastic cordierite in the Grt-Bt gneiss and spinel aggregate in the mafic gneiss are needed, however, those will be reported in a separate paper.

### *8.2. Tectonic significance of the intrusive rocks*

The emplacement of the syenite suite postdates the main metamorphism and deformation event of Filchnerfjella, because the syenite has not undergone any pervasive deformation or metamorphism. Post-tectonic plutonic rocks are widespread in cDML. In Gjelsvikfjella, Ohta *et al.* (1990) determined the time of emplacement of the post deformation charnockite *ca.* 500 Ma by the Rb-Sr whole-rock isochron. U-Pb SHRIMP dating of zircon from post-tectonic syenite (Stabben syenite) that cuts the foliation of migmatites gives an age of 500±19 Ma (Paulsson, 2001). The time of emplacement of the post-tectonic intrusive rocks would, therefore, be *ca.* 500 Ma in cDML (Paech, 2001). The field relationship and petrography of the syenite on Filchnerfjella are similar to those of the post-tectonic pluton rocks from cDML.

The dioritic enclave observed at Trollslottet locally shows quenched texture such as the bladed biotite (Fig. 18b) and includes the host syenite material, suggesting that the magma activity of the dioritic enclave was coeval with that of the syenite. The quartzdiorite and the granite dikes were emplaced after the main metamorphic event

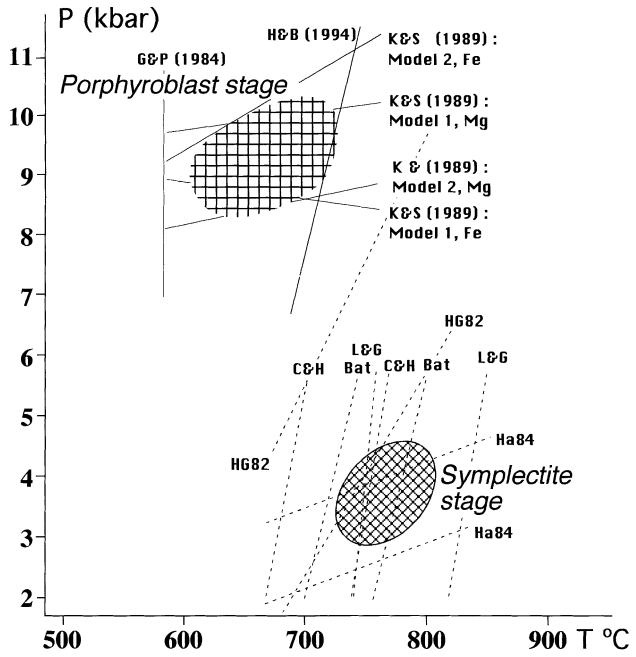


*Fig. 22. Preliminary result of P-T estimates showing the geothermobarometric result (Sample: 02010601B). The porphyroblast stage is deduced from garnet-hornblende-plagioclase-quartz equilibria (Kohn and Spear, 1989: K&S (1989), garnet-hornblende (Graham and Powell, 1984: G&P (1984) and hornblende-plagioclase geothermometer (Holland and Blundy, 1994: H&B (1994)). The Symplectite stage is estimated from the garnet-orthopyroxene geothermometer (Lee and Ganguly, 1988: L&G; Carswell and Harley, 1989: C&H; Battacharya et al., 1991: Bat) and garnet-orthopyroxene-plagioclase-quartz equilibria (Harley, 1984: Ha84; Harley and Green, 1982: HG82).*

because they cut the foliation of the host gneiss and show no signs of metamorphic and deformation textures. In addition, the chemical composition of quartzdiorite is similar to that of the dioritic enclave (Table 3, Fig. 21). The time of the magma activity of the quartzdiorite and the granite dikes, therefore, would be similar to that of the dioritic enclave and also the syenite. The pegmatite and aplite represent the latest magmatic activity in the area.

The intrusive rocks having $SiO_2 \geq 60$ wt% from Filchnerfjella plot around the field of within-plate granites on the discrimination diagram defined by Pearce (1984) (Fig. 23). On the same diagram, the post-tectonic intrusive rocks from Orvinfjella and Wohlthatmassiv, eastern Filchnerfjella, plot in the similar range as the rocks from Filchnerfjella (Fig. 23). Roland (2002) argued that post-tectonic granitoids from Orvinfjella and Wohlthatmassiv were derived from the lower continental crust or underplated crust, and a compressive regime, subduction zone or continent-continent collision, was postulated. The main heat source was considered to be up-welling of the asthenosphere caused by delamination of the continental lithospheric mantle. In this

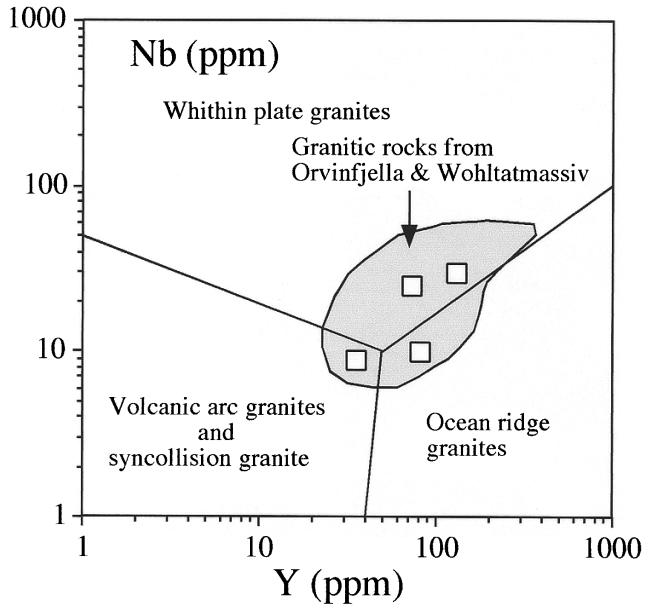


*Fig. 23. After Pearce et al. (1984) Rb vs. Y diagram. The data of the intrusive rocks from Filchnerfjella (this study) and Orvinfjella to Wohlthatmassiv (quoted from Roland, 2002) are plotted around the field of within-plate granite.*

paper, we interpret the dioritic enclave and the quartzdiorite dike as synchronous with the syenite. The quartzdiorite and the dioritic enclave would be differentiated from the more mafic magma derived from the mantle. The trace element pattern of the quartzdiorite and the dioritic enclave are similar to the within plate basaltic rock (Fig. 21). The existence of these mafic rocks strongly supports Roland's (2002) idea that magma underplating from the mantle led to extensive partial melting of the lower crust.

### *8.3. Structural correlation to adjacent regions*

The observed high-grade deformation features can be grouped into different deformation stages. Here, we regard migmatization as the oldest event and the rocks are totally overprinted by the main foliation event. Subsequent deformations affecting the basement gneisses are labelled $D_{n+1}$, containing the oldest recognized structures, and $D_{n+2}$, $D_{n+3}$, etc. for all following events.

Our structural data allow us to distinguish the following events from oldest to youngest: (i) Migmatization; (ii) $D_{n+1}$ (formation of main foliation parallel to compositional layering); (iii) $D_{n+2}$ (isoclinal to tight folding of the main foliation); (iv) $D_{n+3}$ (formation of N- to NNW-vergent open folds and probably co-genetic thrusts); (v) $D_{n+4}$ (low-angle normal faults with S-directed slip); (vi) $D_{n+5}$ intrusion of syenite, granite, etc. and associated pegmatites/aplites; (vii) $D_{n+6}$ (Jurassic basaltic dikes and possibly N-S-directed extensional faulting; (viii) $D_{n+7}$ (Conjugate fault system and co-genetic thrusting due to WNW-ESE-directed maximum horizontal palaeostress).

At present, absolute ages cannot be attributed to the deformation events recorded in the area. In the areas immediately east of Filchnerfjella and Fenriskjeften, at Orvinfjella and Wohlthatmassiv, geochronological studies indicate that polyphase high-grade Pan-African overprint has affected the Grenville-age basement rocks between 580–550 and 530–515 Ma (Jacobs *et al.,* 1998). The latter age cluster is linked to a major phase of extension that led to the intrusion of voluminous late- to post-tectonic migmatites at *ca.* 510 Ma (Mikhalsky *et al.,* 1997). Equivalent Rb-Sr ages around 500 Ma were obtained for plutonic rocks from the western Mühlig-Hofmannfjella (Ohta *et al.,* 1990).We thus tentatively regard at least the events $D_{n+3}$ and $D_{n+4}$ as Pan-African in age. This is well in accordance with the results of Jacobs and Bauer (2001) from Gjelsvikfjella and the western Mühlig-Hofmannfjella. They assumed the presence of large-scale NW-vergent open folds from their structural data. The large-scale Filchnerfjella folds could very well correlate with these structures. Based on the data obtained from Orvinfjella by Jacobs *et al.* (1998), we assume that a Pan-African age may very well be valid also for deformations prior to $D_{n+3}$. The event $D_{n+4}$ could correlate with the aforementioned major extensional phase recorded by these authors. However, to test these hypotheses we plan to perform high-precision U-Pb SHRIMP dating of zircons and other minerals that then may yield reliable data on the age sequence of events.

We thus tentatively regard at least events $D_{n+3}$ and $D_{n+4}$ as pan-African in age. This is well in accordance with the results of Jacobs and Bauer (2001) from Gjelsvikfjella and the western Mühlig-Hoffmannfjella. They assumed the presence of large-scale NW-vergent open folds from their structural data. The large-scale Filchnerfjella folds could very well correlate with these structures. Based on the data from Orvinfjella by Jacobs *et al.* (1998), we assume that a pan-African age may very well be valid also for deformations prior to $D_{n+3}$. The event $D_{n+4}$ could correlate with the aforementioned major extensional phase recorded by these authors. This interpretation is underlined by the fact that $D_{n+3}$-structures (i) overprint high-grade rocks with (most likely) pan-African metamorphism and (ii) crosscut by late-/post-pan-African aplites. To test these hypotheses we plan to perform high-precision U-Pb SHRIMP dating of zircons and other minerals, which then may yield reliable data on the age sequence of events.

The latest, brittle to semi-ductile, deformation events $D_{n+5}$ and $D_{n+6}$ can clearly be attributed to the break-up and fragmentation of the supercontinent Gondwana. An older, only locally preserved N-S directed extensional event seems to be genetically linked to basaltic dikes preserved in WSW-ENE trending faults. These dikes are most likely Jurassic in age and result from the initial break-up of Gondwana. The subsequent conjugate system and associated thrusts, which overprint these older features, are difficult to date. However, some conclusions can be drawn from field relations and some geochronology data: (i) The faults overprint the Pan-African intrusions and are thus post-Pan-African in age; (ii) They overprint extensional faults and Jurassic dikes and are hence post-Jurassic; (iii) The brittle faults disrupt the old, likely Permian (Lisker, pers. comm.) denudational surface and are thus as old or younger than an uplift phase disrupting this surface. Fission track data from Dronning Maud Land indicate that a major uplift phase occurred in Cretaceous times (Jacobs and Lisker, 1999). The

faults recorded in the expedition area are thus at least Late Cretaceous or Cenozoic in age.

## Acknowledgments

The field survey was supported by the Ministry of Education, Culture, Sports, Science and Technology, National Institute of Polar Research, the Norwegian Polar Institute, and the German Alfred-Wegener-Institute for Polar and Marine Research. We express our sincere thanks to our field guide Mr. Ian Manson and the members of NARE 2001/2002 for their helpful support during the field season, and to Prof. Y. Ohta for valuable discussions. We thank Dr. G.H. Grantham and an anonymous referee for critically assessing the manuscript. Additional funding from the Japan Society for Promotion of Science to S.B. is gratefully acknowledged. A.L. and J.J. wish to thank the Deutsche Forschungsgemeinschaft for financial support (grants La 1080/2–1 and Ja 617/21–1).

## References

Austrheim, H., Elvevold, S., Engvik, A.K. and Paulsson, O. (1997): Geological observations in Gjelsvikfjella, Mühlig-Hofmannfjella and western Orvinfjella during NARE 96/97. Nor. Polarinst. Medd., **148**, 77–84.

Battacharya, A., Krishnakumar, K.R., Raith, M. and Sen, S.K. (1991): An improved set of a-X parameters for Fe-Mg-Ca garnets and refinements of the orthopyroxene-garnet thermometer and the orthopyroxene-garnet-plagioclase-quartz barometer. J. Petrol., **32**, 629–656.

Bucher-Nurminen, L. and Ohta, Y. (1993): Granulites and garnet-cordierite gneiss from Dronning Maud Land, Antarctica. J. Metamorph. Geol., **11**, 691–703.

Carswell, D.A. and Harley, S.L. (1989): Mineral thermometry and barometry. Eclogite Facies Rocks, ed. by D.A. Carswell. Glasgow, Blackie and Sons, 83–110.

Chester, F.M. and Logan, J.M. (1987): Composite planar fabric of gouge from the Punchbowl Fault, California. J. Struct. Geol., **9**, 621–634.

Cox, K.G., Bell, J.D. and Pankhurst, R.J. (1979): The Interpretation of Igneous Rocks. London, George, Allen and Unwin, 450 p.

Dallmann, W.K., Austrheim, H., Bucher-Nurminen, K. and Ohta, Y. (1990): Geology around the Norwegian Antarctic station "Troll", Jutulessen, Dronning Maud Land. Nor. Polarinst. Medd., **111**, 39 p.

Jacobs, J. and Bauer, W. (2001): Gjelsvikfjella and Mühlig-Hofmann-Gebirge (E-Antarctica): Another piece of the East Antarctic Orogen? Z. dt. Geol. Ges., **152**, 249–259.

Jacobs, J. and Lisker, F., (1999): Post Permian tectono-thermal evolution of western Dronning Maud Land, E-Antarctica: an apatite fission-track approach. Antarct. Sci., **11**, 451–460.

Jacobs J., Fanning C.M., Henjes-Kunst F. Olesch M. and Paech H.-J. (1998): Continuation of the Mozambique Belt into East Antarctica: Grenville-Age Metamorphism and Polyphase Pan-African High-Grade Events in Central Dronning Maud Land. J. Geol., **106**, 385–406.

Graham, C.M. and Powell, R. (1984): A garnet-biotite geothermometer: calibration, testing, and application to the Pelona Schist, southern California. J. Metamor. Geol., **2**, 13–21.

Grantham, G.H., Jackson, C., Moyes, A.B., Groenewald, P.B., Harris, P.D., Ferrar, G. and Krynauw, J.R. (1995): The tectonothermal evolution of the Kirwanveggen－H.U. Sverdrupfjella areas, Dronning Maud Land, Antarctica. Precamb. Res., **18**, 2–10.

Harley, S.L. (1984): The solubility of alumina in orthopyroxene coexisting with garnet in FeO-MgO-$Al_2O_3$-$SiO_2$ and CaO-MgO-$Al_2O_3$-$SiO_2$. J. Petrol., **25**, 665–696.

Harley, S.L. and Green, D.H. (1982): Garnet-orthopyroxene barometry for granulites and peridotites. Nature, **300**, 697–701.

Hanmer, S. and Passchier, C.W. (1991): Shear-sense indicators: a review. Geol. Surv. Canada, Paper **90–17**, 1–72.

Holland, T.J.B. and Blundy, J.D. (1994): Non-ideal interactions in calcic amphiboles and their bearing on amphibole plagioclase thermometry. Contrib. Mineral. Petrol., **116**, 433–447.

Kohn, M.J. and Spear, F.S. (1989): Emprical calibration of geobarometers for the assemblage garnet-hornblande-plagioclase-quartz. Am. Mineral., **74**, 77–84.

Lee, H.Y. and Ganguly, J. (1988): Equilibrium compositions of coexisting garnet and orthopyroxene: reversed experimental determinations in the system FeO-MgO-$Al_2O_3$-$SiO_2$ and applications. J. Petrol., **29**, 93–114.

Mikhalsky, E.V., Beliatsky, B.V., Savva, E.V., Wetzel, H.-U., Fedorov, L.V., Weiser, T. and Hahne, K. (1997): Reconnaissance geochronologic data on polymetamorphic and igneous rocks of the Humboldt Mountains, Central Dronning Maud Land, East Antarctica. The Antarctic Region: Geological Evolution and Progresses, ed. by C.A. Ricci. Siena, Terra Antarctica Publication, 45–54.

Moyes, A.B. (1993): The age and origin of the Jutulsessen granitic gneiss, Gjelsvikfjella, Dronning Maud Land. S. Afr. J. Antarct. Res., **23**, 25–32.

Näslund, J.O. (1997): Airborne radar soundings of ice depth, GPS measurements of ice velocity and studies of landform evolution in Central Dronning Maud Land, East Antarctica. Nor. Polarinst. Medd., **148**, 125–136.

Otha, Y. (1999): Nature Environment map, Gjelsvikfjella and Western Mühlig-Hofmannfjella, sheets 1 and 2, Dronning Maud Land, East Antarctica. 1:100,000. Norsk Polarinstitutt, Temakart Nr. **24**.

Ohta, Y., Tørudbakken, B. and Shiraishi, K. (1990): Geology of Gjelsvikfjella and Western Mühlig-Hofmannfjella, western Dronning Maud Land, East Antarctica. Polar Res., **8**, 99–126.

Paech, H.J. (2001): Pervasive Pan-African reactivation of the Grenvillian crust and large igneous intrusions in central Dronning Maud Land, East Antarctica. Continental Reactivation and Reworking, ed. by J.A. Miller *et al.* London, Geol. Soc., 343–355 (Geol. Soc. Lond. Spec. Pub1., 184).

Passchier, C.W. and Trouw, R.A.J. (1996): Microtectonics. Berlin, Springer, 289 p.

Paulsson, O. (2001): Geochronology and geochemistry of the rocks at the Jutulessen nunataks, Dronning Maud Land, Antarctica. Abstract EUG11.

Pearce, J.A., Harris, N.B.W. and Tindle, A. (1984): Trace element discrimination diagrams for the tectonic interpretation of granitic rocks. J. Petrol., **25** 956–983.

Petit, J.P. (1987): Criteria for the sense of movement on fault surfaces in brittle rocks. J. Struct. Geol., **9**, 597–608.

Ravich, M.G. and Krylov, A.Y. (1964): Absolute ages of rocks from East Antarctica. Antarctic Geology, ed. by R.J. Adie. Amsterdam, North Holland Publ., 590–596.

Roland, N.W. (2002): Pan-African granitoids in central Dronning Maud Land, East Antarctica: petrography, geochemistry, and plate tectonic setting. R. Soc. N. Z. Bull., **35**, 85–91.

Sakiyama, T., Takahashi, Y. and Osanai, Y. (1988): Geological and petrological characters of the plutonic rocks in the Lunckeryggen-Brattnipene region, Sør Rondane Mountains, East Antarctica. Proc. NIPR Symp. Antarct. Geosci., **2**, 80–95.

Shiraishi, K., Asami, M. and Kanaya, H. (1983): Petrochemical character of the syenitic rocks from the Yamato Mountains, East Antarctica. Mem. Natl Inst. Polar Res., Spec. Issue, **28**, 183–197.

Shiraishi, K., Asami, M., Ishizuka, H., Kojima, H., Kojima, S., Osanai, Y., Sakiyama, T., Takahashi, Y., Yamazaki, M. and Yoshikura, S. (1991): Geology and metamorphism of the Sør Rondane Mountains, East Antarctica. Geological Evolution of Antactica, ed. by M.R.A. Thomson *et al.* Cambridge, Cambridge University Press, 77–82.

Stern, R.J. (1994): Arc assembly and continental collision in the Neoproterozoic East African Orogen: Implications for the consolidation of Gondwana. Earth Planet. Sci. Rev., **22**, 319–351.

Tainosho, Y., Takahashi, Y., Arakawa, Y., Osanai, Y., Tsuchiya, N., Sakiyama, T. and Owada, M. (1992): Petrochemical character and Rb-Sr isotopic investigation of the granitic rocks from the Sør Rondane Mountains, East Antarctica. Recent Progress in Antarctic Earth Science, ed. by Y. Yoshida *et al.* Tokyo, Terra Sci. Publ., 45–54.